Quantitative Phase Microscopy: how to make phase data meaningful

Goldie Goldstein[1] and Katherine Creath[1,2,3*]
[1]4D Technology Corporation, Tucson AZ 85706,
[2]College of Optical Sciences, The University of Arizona, Tucson, AZ USA 85721 and,
[3]Optineering, Tucson, AZ USA 85719

ABSTRACT

The continued development of hardware and associated image processing techniques for quantitative phase microscopy has allowed superior phase data to be acquired that readily shows dynamic optical volume changes and enables particle tracking. Recent efforts have focused on tying phase data and associated metrics to cell morphology. One challenge in measuring biological objects using interferometrically obtained phase information is achieving consistent phase unwrapping and background shape removal throughout a sequence of images. Work has been done to improve the phase unwrapping in two-dimensions and correct for temporal discrepanices using a temporal unwrapping procedure. The residual background shape due to mean value fluctuations and residual tilts can be removed automatically using a simple object characterization algorithm. Once the phase data are processed consistently, it is then possible to characterize biological samples such as myocytes and myoblasts in terms of their size, texture and optical volume and track those features dynamically. By observing optical volume dynamically it is possible to determine the presence of objects such as vesicles within myoblasts even when they are co-located with other objects. Quantitative phase microscopy provides a label-free mechanism to characterize living cells and their morphology in dynamic environments, however it is critical to connect the measured phase to important biological function for this measurement modality to prove useful to a broader scientific community. In order to do so, results must be highly consistent and require little to no user manipulation to achieve high quality nynerical results that can be combined with other imaging modalities.

Keywords: phase imaging, interference microscopy, polarization interferometry, cellular imaging, cell dynamics, optical thickness measurement

1. INTRODUCTION

A quantitative phase microscope (QPM) has been prototyped capable of instantaneously measuring live cells. It allows the ability to follow motions and processes over time, quantifying such things as cellular dynamics, motility, and cell and tissue morphology. Phase imaging quantifies optical thickness variations due to small variations in refractive index relating to variations in density of different structures and materials within cells and tissues. Very small refractive index variations can manifest as large variations in optical thickness. This paper presents an update on research in developing analysis methods for this microscope and shares recent measured results. The conversion of raw measurements into useful and consistent phase information is the critical step that determines accuracy and usefulness of quantitative phase microscopy. Further connecting the measured phase to biological function is vital to help educate the broader scientific community and in turn make the QPM a more useful and versatile tool to study cellular morphology dynamics. Consistent, high-quality phase data is easily obtained with the methods explored in this work and is capable of enabling the scientific community to more readily explore the power of this extremely sensitive label-free imaging technique.

2. BACKGROUND

Techniques developed for full-field phase-imaging interference microscopes have historically relied upon temporal phase-measurement methods, which obtain interferograms sequentially at multiple time points; this requires vibration isolation and limits acquisition speeds based on the number of camera frames to be processed. [1-3] The method utilized in this microscope developed by 4D Technology relies on a pixelated polarization mask with a low coherence source to obtain high quality phase measurements in one snapshot. This enables data acquisition at rates up to 15 images per second and

* email: goldie.goldstein@4dtechnology.com

Three-Dimensional and Multidimensional Microscopy: Image Acquisition and Processing XXI,
edited by Thomas G. Brown, Carol J. Cogswell, Tony Wilson, Proc. of SPIE Vol. 8949, 89491C

eliminates the need for vibration isolation to obtain high quality images. The design of this microscope has been described previously and more detail can be found in the literature. [4]

2.1 Dynamic interference microscope system

The quantitative phase microscope used for this work is a Linnik-based configuration. It consists of a Köhler-type illumination system utilizing a low coherence extended source, [5] and a simple imaging system as shown in Figure 1. An aperture stop enables controlling the size of the source in the entrance pupil of the microscope objectives, while a field stop enables easier alignment of the system.

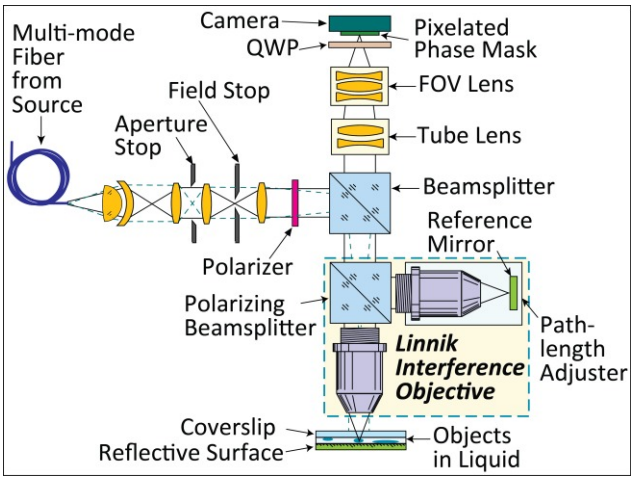

Figure 1. Optical schematic of Linnik interference microscope

The object and reference beams have orthogonal linear polarizations with the incoming illumination split before the microscope objectives using a polarization beamsplitter. The relative irradiances of the test and object beam are balanced for maximum contrast by changing the angle of the linear polarizer. A quarter-wave plate (QWP) before the camera combines the two polarized beams so that they can interfere at the pixelated phase mask. For the measurements in this paper, samples in water or cell media are viewed in reflection through a cover slip. Sources with wavelengths of 515nm, 660 nm and 785 nm were used with a 50X NA 0.8 or 20X NA 0.45 microscope objective. The imaging tube lens magnification is 1X with a flip-in 2.25X field of view (FOV) lens.

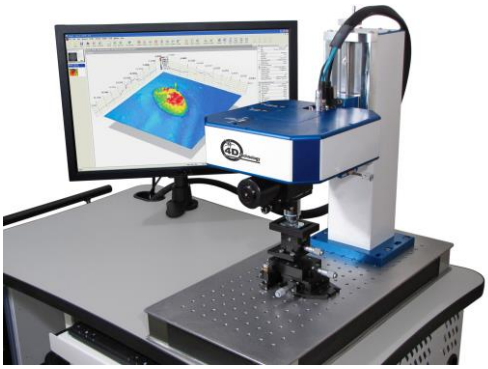

Figure 2. Prototype interference microscope.

Figure 2 shows a photograph of the prototype system. The Linnik objective is seen below the microscope (blue and white box) with a 5-axis translation stage below for adjusting position and tip/tilt of the sample. The compact design of this system enables it to be used on a variety of stands so that it can be interfaced with different types of staging and cell handling systems.

2.2 Obtaining phase images and determining optical thickness

For phase imaging applications, pixelated phase mask sensor technology uniquely provides a single frame phase measurement in a compact, robust format that is compatible with conventional microscope imagining systems, and permits the use of a wide variety of wavelengths and source bandwidths without the need for vibration isolation or scanning.[6-8] All necessary information to determine phase is recorded in a single snapshot. It enables the creation of a versatile and compact microscope interferometer for biological applications.

2.2.1 Wire-grid polarizers

The polarization-mask is constructed from an array of micropolarizers that are constructed from wire grid polarizers as shown in Figure 3. Wire-grid polarizers are made of tiny metal wires that are deposited on a transparent substrate (typically aluminum wires on a glass substrate). The linewidth, thickness and period of the wires are approximately 100nm, 120nm and 240nm respectively**.** These sub-wavelength structures have the property of reflecting light polarized parallel to the wires and transmitting light polarized perpendicular to them. They function as efficient polarizers over a wide range of wavelengths and angles.

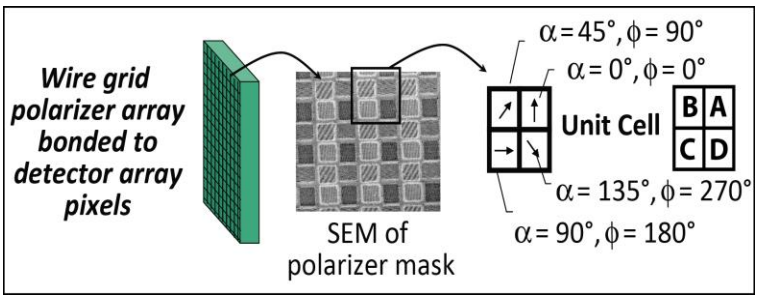

Figure 3. The pixelated phase mask has 4 different polarizations comprising a unit cell of 2x2 different relative phase values.

2.2.2 Phase imaging with a pixelated phase-mask

At the phase mask, the reference and test beams have orthogonal circular polarizations (i.e., right-hand circular and left-hand circular). When combined, the measured irradiance at each pixel of the mask is given by Equation (1). [9]

$$I(x,y) = \frac{1}{2}\{I_r + I_s + 2\sqrt{I_r I_s}cos[\Delta\varphi(x,y) + 2\alpha_p]\}, \quad (1)$$

where α_p is the angle of the polarizer with respect to the x, y plane, I_r and I_s are the intensity of reference and signal beams respectively, and $\Delta\phi(x,y)$ is the optical path difference between the beams. When this equation is applied to each of the 4 pixels in the unit cell, phase differences of 0°, 90°, 180°, and 270° are encoded into a single image when a single interferogram is recorded. For each of the four pixel types we can write Equations (2)-(5) as,

$$A(x,y) = \frac{1}{2}\{I_r + I_s + 2\sqrt{I_r I_s}cos[\Delta\varphi(x,y)]\} \quad (2)$$

$$B(x,y) = \frac{1}{2}\left\{I_r + I_s + 2\sqrt{I_r I_s}cos\left[\Delta\varphi(x,y) + \frac{\pi}{2}\right]\right\} \quad (3)$$

$$C(x,y) = \frac{1}{2}\{I_r + I_s + 2\sqrt{I_r I_s}cos[\Delta\varphi(x,y)] + \pi\} \quad (4)$$

$$D(x,y) = \frac{1}{2}\left\{I_r + I_s + 2\sqrt{I_r I_s}cos\left[\Delta\varphi(x,y) + \frac{3\pi}{2}\right]\right\}. \quad (5)$$

Four simultaneous full-field interferograms can then be synthesized by combining pixels of each phase type. These four interferograms can be processed by a variety of algorithms that are well-known for calculating image phase.[10, 11] One well-known phase algorithm is the simple four-frame algorithm shown in Equation (6) as,

$$\psi(x,y) = ATAN2[D(x,y) - B(x,y), A(x,y) - C(x,y)], \quad (6)$$

where ATAN2 is the 2π arctangent function. This produces a modulo 2π (wrapped) phase map which then needs to be unwrapped.

2.3 Unwrapping the phase in space and time

The result of Equation 6 is the wrapped phase which must be unwrapped so it is no longer restricted on the range $-\pi<\psi\leq\pi$ radians. The unwrapped phase estimate will be generally referred to as φ. Phase unwrapping is a topic that has been discussed at length, both in terms of unwrapping algorithms and also in performance comparisons. [12-15] For this work, a quality-guided modulation-based phase unwrapping algorithm was implemented.[12] Despite using such a robust phase unwrapping algorithm, inconsistencies still exist in the unwrapped phase results among frames of data as seen in the rotifer imaged in Figure 4.

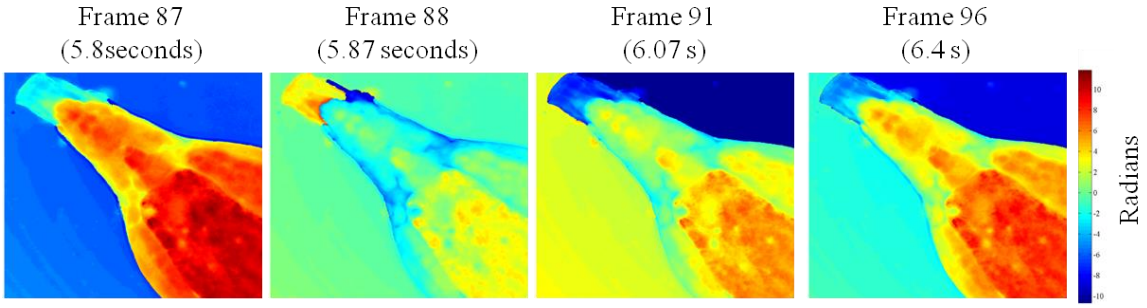

Figure 4: Rotifer showing inconsistent phase unwrapping between four frames of measurement data.

This figure shows four different unwrapping results for nearly the same wrapped phase. Mutliple sources of error that can negatively impact the captured interferograms and their conversion into unwrapped phase are: noise, low modulation, object discontinuities, and violation of sampling theorem [16]. Because the absolute phase information of the rotifer in Figure 4 is unknown, assumptions must be made about the nature of the sample and whether or not the resultant unwrapped phase is realistic. For this measurement, the most realistic unwrapped phase for the four frames presented in the above figure is that of Frame 87 (far left). The two separate background regions on each side of the rotifer are unwrapped to approximatley the same phase value. The body of the rotifer is unwrapped such that the transition from the thin regions of the tail (top left corner) to the central body region increases. Lastly, the background optical thickness is less than that of the rotifer which leads to the conclusion that the measurement is reaslistic. The difficulty in real measurements is that phase unwrapping inconsistencies can be detrimental to quantitative analysis. A method is desired that can unwrap the phase shown in Figure 4 consistently throughout the sequence of data.

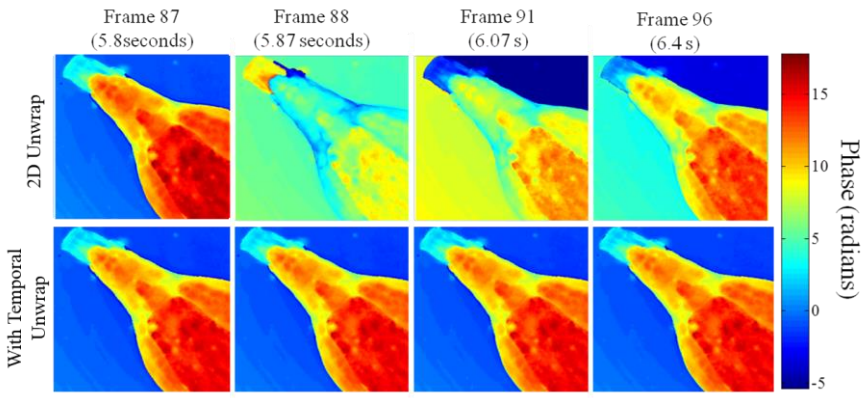

Figure 5: Comparison of two-dimensional phase unwrapping with additional temporal unwrapping. The temporal unwrapping step makes these frames of data usable.

Consistent two-dimensional phase unwrapping in a dataset is critical for accurate quantization of metrics such as optical thickness or volume of a dynamic observation. Without it, inconsistent frames of data must be discarded since the information they provide is not consistent with the rest of the dataset. Strategies exist for other applications outside of interferometry, such as MRI and InSAR, to consistently unwrap three-dimensional phase data with significant interframe motion. [17-19] Simpler approaches can be taken by temporally unwrapping the data and assuming minimal motion [20,

21]. In this case, the assumption is that there is minimal phase aliasing in the temporal axis. For the analysis of data acquired by the QPM, methods must be developed that specifically apply to the phase data and create consistency within datasets. By first two-dimensionally phase unwrapping each frame of data, then subsequently applying a temporal phase unwrapping algorithm, it is possible to reduce interframe unwrapping errors. Without these methods, frames of data with inconsistent phase unwrapping must be thrown out. When observing biological phenomenon, having the greatest quantity of data with the highest time resolution is preferred. Intelligent application of two-dimensional and temporal phase unwrapping in combination provide a good solution for consistent phase measurement.

Although the unwrapped phase is now consistent between sequential frames of data, there is often residual background shape due to measurements in the interferometer being made in a non-null condition. Strategies to reduce the presence of this background shape is a crucial next step in data processing for quantitative phase microscopy.

2.4 Automated Background removal

The goal is to have the phase measurement of an object of interest not to be influenced by variations in the measurement condition (e.g. coverglass thickness variations, slight mirror deviations, alignment error, vibration, etc). Within the field of quantitative phase microscopy, background fluctuations are problematic for several reasons. When there is tilt between the reference and test arm of the interferometer (Linnik objective in this case), the cells appear to have the wrong thickness. Additionally, fluctuations in the mean value of the data results in temporal optical thickness changes that are inaccurate and prevent calculation of dry cell mass, optical volumes, or other important parameters used for scientific utility.

The background fluctuations are largely due residual vibration which is present whether or not the system is vibrationally isolated, but is magnified for systems placed on a standard workbench. This residual vibration causes small fluctuations in the mean value of the phase data. The second factor is the residual background shape due to non-null measurement configuration (residual tilt fringes and potentially higher order terms). In addition, there are also persistent and systematic optical deviations within the interferometer that can be removed by making a reference measurement. This is a well-known technique used in interferometry to remove optical aberrations characteristic to the interferometer and remove them from the measurement. [22] Residual background shape due to environmental changes and alignment errors can be removed manually or automatically as is shown in Figure 6. By isolating the background and forcing its mean value to be consistent across several frames of data, phase measurements can be made relative to the background with increased accuracy. [23] The importance of the background shape removal lies in the assumption that the accuracy of a phase measurement of a feature of interest is limited by the phase stability of the background.

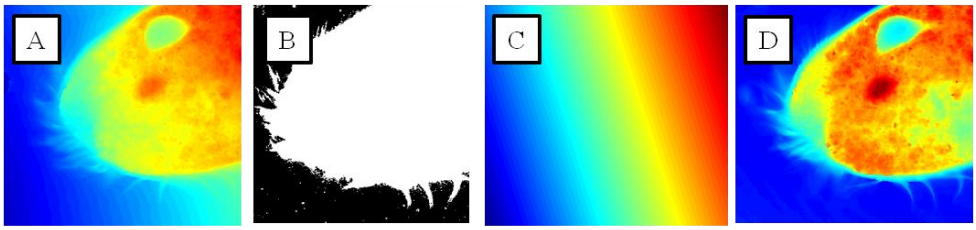

Figure 6: Automatic background applied to paramecium dataset shows (A) the unwrapped phase, (B) the mask created to find the background, (C) the best fit surface to the background and (D) the residual background leveled phase.

2.5 Determining optical thickness and optical volume

Now that a consistently unwrapped, background leveled version of the measured phase is available, it can be discussed in either phase (radians) or in terms of wavelengths of the source light (waves or nm). The phase data can be converted to optical thickness OT(x,y) as shown in Equation (7) as,

$$OT(x,y) = OPD \cdot \frac{\lambda}{2} = \varphi(x,y)\left[\frac{\lambda}{4\pi}\right] \tag{7}$$

Optical thickness (OT), seen in Equation (8), is an integrated measure of the overall optical path through the sample, which is the product of the localized index of refraction n(x,y,z) and the physical thickness t(x,y,z),

$$OT(x,y) = \int_0^T n(x,y,z) \cdot t(x,y,z)dz. \tag{8}$$

For viewing in reflection OT includes a double pass through the coverslip and liquid containing the objects. Denser areas of the object with higher indices of refraction will yield a larger OT as shown in Figure 7.

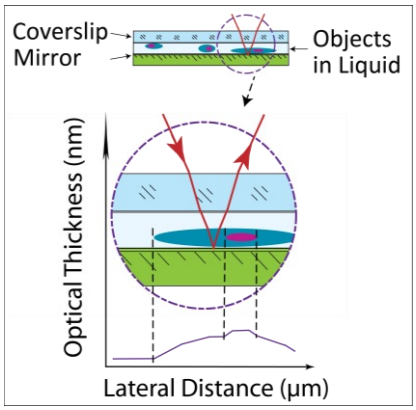

Figure 7. Optical path length through test sample includes the coverslip, liquid and objects. Graph (bottom) shows optical thickness profile for the section within the highlighted area.

Optical volume can also be calculated by integrating the optical thickness over a finite field of view. This quantity can provide additional valuable information to the scientific community. For this work, optical volume (OV) is being defined in Equation (9) as,

$$OV(\tau) = \int_{y_1}^{y_2} \int_{x_1}^{x_2} \int_0^{\tau} n(x,y,z) \cdot t(x,y,z) dz\, dx\, dy \tag{9}$$

This is equivalent to the optical thickness integrated over an area of the field of view for each frame captured at time τ. The importance in measuring optical volume is that it is proportional to dry cell mass, which can be used to measure growth and changes within a cell during its life cycle. [24-29] Quantitative phase microscopy is a very sensitive tool to investigate small changes in optical volume. By using a QPM to observe dynamic bioogical processes, it is possible to observe very small relative changes in optical thickness of a sample.

3. SAMPLE MEASUREMENTS

The value in quantitative phase measurements comes with the further analysis of the acquired data. There are many ways to analyze the data and extract additional information from the quantitative phase information. One simple quantitative exploration is characterizing cell size over time. Cellular boundaries are easily extracted using quantitative phase data. It is also possible to observe optical volume of a region as a function of time to observe changes, such as strength of contractions in spontaneously beating myocytes. Cell boundary identification can provide morphological characterization of difference cell types. Ultimately, this type of analysis can help tie functional changes to morphological changes.

3.1 Cellular Morphology Dynamics

Quantitative phase data enables the fast labeling of cells from their surrounding media. The size of a cell can quickly and effectively be characterized over the course of a measurement. Myocytes were measured over a period of 1:20 hours. Their boundaries were characterized using standard methods and the resultant cell is shown in Figure 8. [30]

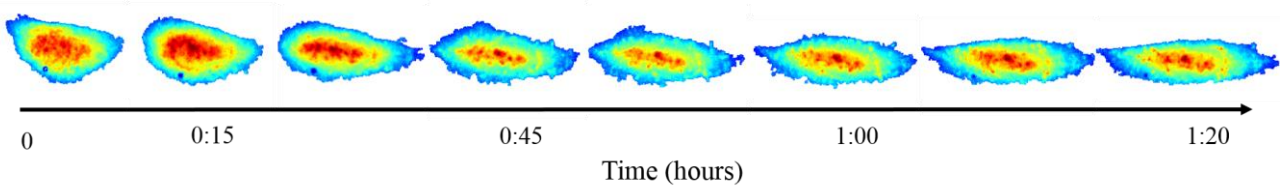

Figure 8: Cell boundary of myocytes

By first defining the cellular boundaries, it is then possible to extract more information from the dataset by characterizing the region of interest using many different tools. As is true in phase contrast measurements, the cellular extent as well as

size in the major and minor axes of the cells can be recorded. This is shown in Figure 9. There are other morphological metrics that can be measured once cellular boundaries are identified. The optical volume can be recorded and tracked to track cellular growth or to study the emission of intracellular particles. Further image analysis can determine texture parameters relating to the cell optical thickness. With this instrument, it is possible to observe and potentially quantify phenomena such as cell membrane ruffling as cells are moving and morphing.

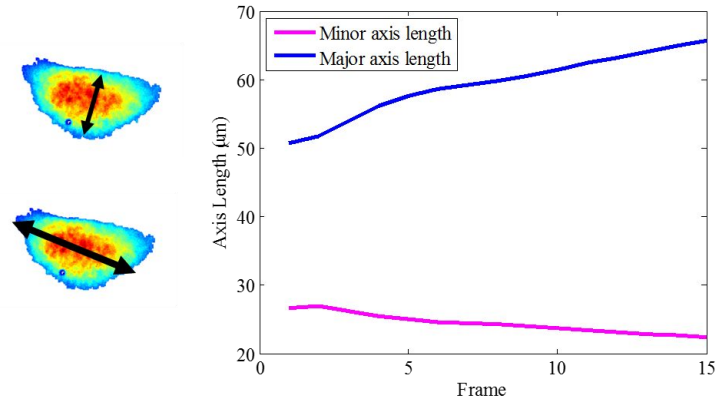

Figure 9: Major and minor axes length of Myocytes measured over 1 hour 20 minutes.

Because QPM is still gaining momentum in the scientific community, it is important to show that these cellular measures, such as size, can be consistently measured over time. By confirming these results are consistent among different imaging modalities, it is a preliminary step in proving that label free imaging provides similar measurement of cellular extent as traditional imaging techniques. The next and most critical step is to further link quantitative phase information to cellular function to continue to show its effectiveness as a new and useful tool for the study of dynamic living organisms.

3.2 Optical Volume Dynamics

Observing optical volume dynamics is a tool that is made possible through consistent dynamic QPM results. Rat cardiac myocytes cultured onto a coverslip were observed at 15 fps. The phase data was unwrapped and background shape was removed. Two frames of optical thickness data are shown in Figure 10, before and after the application of IPHC (isoproterenol hydrochloride), a drug that increases beating frequency.

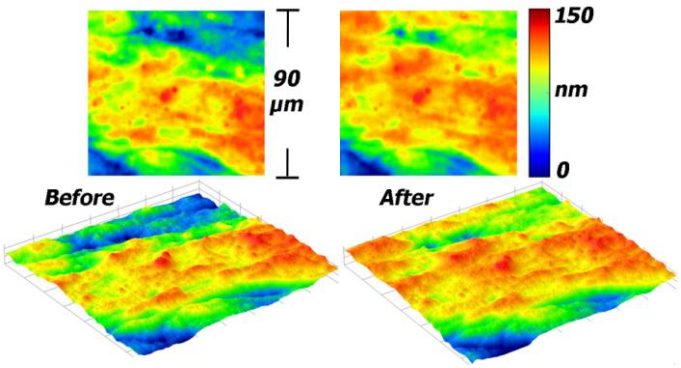

Figure 10: Rat Cardiac Myocytes show before (left) and after (right) the application

For the field of view shown, the optical volume can be calculated using Equation 9 for each measured point in time. The relative optical volume changes are seen in Figure 11.

By observing relative changes in optical volume over time, it is possible to observe two distinct results of applying IPHC to the myocytes: 1) the beating frequency increases by approximately a factor of eight, and 2) the beating strength increases by a factor of three. Characterization of beating strength is one example where quantitative phase microscopy provides information that is not obtainable through any other known observation method.

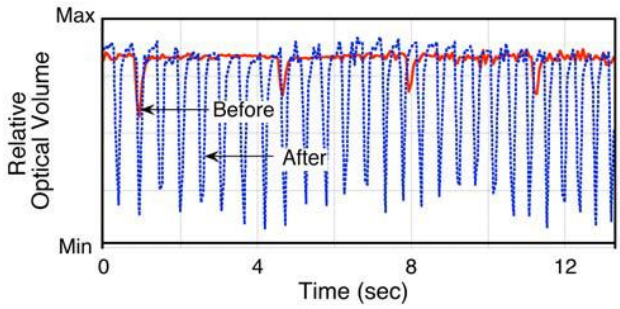

Figure 11: Beating rat cardiac myocytes optical volume shown before (red) and after (blue) application of IPHC, a drug intended to induce increased beating frequency.

Another case in which quantitative observations of optical volume can be achieved is in the observation of vesicles travelling along actin fibers within myoblasts. By tracking two clusters of vesicles, the optical volume can be observed as these two clusters join together. Under phase contrast or brightfield microscope images, once two particles overlap one another, they can no longer be distinguished from each other. Using QPM, the optical volume of the vesicles allows for location tracking, even when particles overlap. Myoblasts were measured every minute over the course of 15 minutes. Two clusters were identified to track that cluster together during the course of the measurement, as seen in Figure 12.

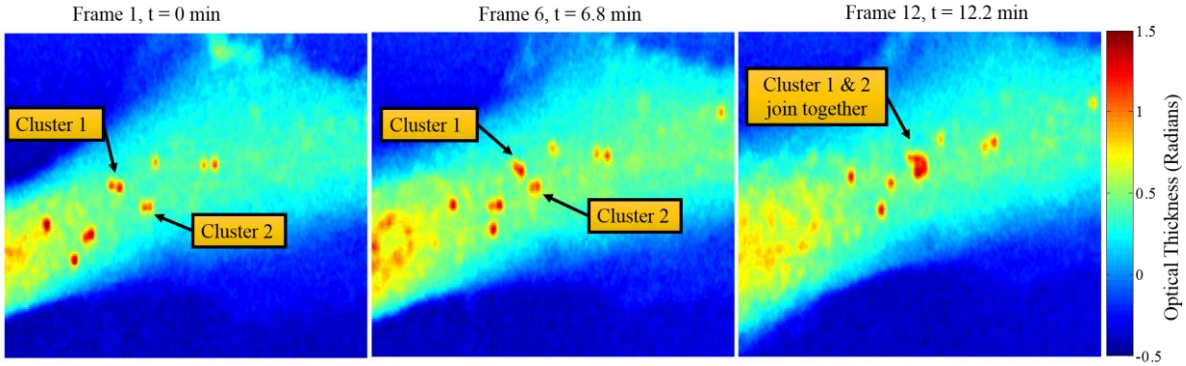

Figure 12: Myoblasts with Cluster 1 and 2 being tracked as they begin to merge, taken at 40X, FOV = 45µm

These two clusters were then tracked and their optical volume calculated at each measurement point as they move towards one another and then become indistinguishable. The relative optical volume is shown in Figure 13.

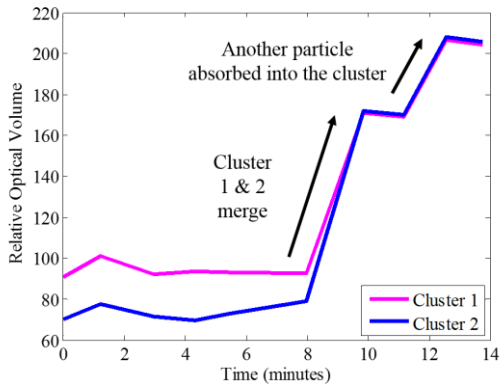

Figure 13: Relative Optical Volume of Myoblast vesicles

As cluster 1 and 2 merge, their relative optical volume values effectively sum. The individual optical volume of cluster 1 and 2 compared to their optical volume once they merge agrees to within 0.4%. In addition, it is possible to see a discernable jump in the optical volume as another particle is absorbed into the cluster at 12 minutes. The consistent summation of the optical volume as two clusters merge provides evidence that quantitative phase measurements are sensitive and accurate even when particles start to overlap. If their individual optical volumes are known at some point in the measurement, estimates can be made regarding their position and group contribution when they become indistinguishable from other features within a measurement.

4. DISCUSSION AND CONCLUSIONS

This paper updates the progress of the development of a QPM and the correpsonding image processing techniques necessary to retrieve consistent and accurate quantification of phase data describing cellular morphology dynamics. The image processing necessary to convert the raw phase data into a useful stream of data is non-trivial. Two-dimensional phase unwrapping techniques have been coupled with temporal phase unwrapping to create consistent dynamic phase measurements. Background leveling techniques are applied to minimize mean value fluctuations and residual tilts from environmental fluctuations. The elimination of the background variation is critical to measurement accuracy. With processed datasets, it is possible to easily identify cellular boundaries and in turn, characterize these local regions with metrics such as their size, local curvature, texture and optical volume. Particles, such as vesicles within myoblasts were tracked and it was shown that the optical volume of overlapping particles agrees to the individual particle's optical volume within 0.4%. This level of agreement implies that particle tracking is still possible even if overlap starts to occur. The analysis examples shown in this work exemplify only a small fraction of the kinds of information that can be realized from quantitative phase data. Efforts are ongoing to find additional metrics that further display the utility of phase information in biology.

5. ACKNOWLEDGEMENTS

The authors wish to thank 4D Technology colleagues Tim Horner and Mark McKune for design of the Linnik and prototype interferometer, Richard Robinson for electrical design, Neal Brock for new technology development, Charles Crandall for software, and James Millerd as co-PI on this project. We also wish to thank Dr. Andrew Rouse, Dr. Ronald Lynch, Jordan Lancaster, and Craig Weber of The University of Arizona Department of Radiology for cell samples. This work was partially supported by NIH/NCRR 1R43RR028170-01, 2R44RR028170-02, and NIH/NIGMS 8R44GM103406-03.

6. REFERENCES

[1] Sommargren, G. E., "Optical Heterodyne Profilometry," Applied Optics 20, 610-618 (1981).
[2] Wyant, J. C., Koliopoulos, C. L., Bhushan, B. *et al.*, "An optical profilometer for surface characterization of magnetic media," ASLE Trans. 27, 101-113 (1984).
[3] Schmit, J., Creath, K., and Wyant, J. C., [Ch. 15. Surface Profilers, Multiple Wavelength, and White Light Interferometry] Wiley-Interscience, Hoboken, N.J.(2007).
[4] Creath, K., and Goldstein, G., "Dynamic quantitative phase imaging for biological objects using a pixelated phase mask," Biomed. Opt. Express 3(11), 2866-2880 (2012).
[5] Born, M., and Wolf, E., [Principles of Optics] Pergamon Press, Oxford(1975).
[6] Brock, N. J., Millerd, J. E., Wyant, J. C. *et al.*, [Pixelated phase-mask interferometer] 4D Technology Corporation, United States(2007).
[7] Kimbrough, B. T., "Pixelated mask spatial carrier phase shifting interferometry algorithms and associated errors," Applied Optics 45(19), 4554-4562 (2006).
[8] Novak, M., Millerd, J., Brock, N. *et al.*, "Analysis of a micropolarizer array-based simultaneous phase-shifting interferometer," Applied Optics 44(32), 6861-6868 (2005).
[9] Kothiyal, M. P., and Delisle, C., "Shearing interferomter for phase-shifiting interferometry with polarization phase-shifter," Applied Optics 24(24), 4439-4442 (1985).
[10] Creath, K., [Phase-measurement interferometry techniques] Elsevier Science Publishers, Amsterdam(1988).
[11] Malacara, D., ServÌn, M., and Malacara, Z., [Interferogram analysis for optical testing] Taylor & Francis, Boca Raton, FL(2005).

[12] Ghiglia, D. C., and Pritt, M. D., [Two-dimensional phase unwrapping : theory, algorithms, and software] Wiley, New York(1998).
[13] Malacara, D., [Optical Shop Testing] Wiley-Interscience, Hoboken, N.J., 623-629 (2007).
[14] Zebker, H. A., and Lu, Y., "Phase unwrapping algorithms for radar interferometry: residue-cut, least-squares, and synthesis algorithms," J. Opt. Soc. Am. A 15(3), 586-598 (1998).
[15] Zappa, E., and Busca, G., "Comparison of eight unwrapping algorithms applied to Fourier-transform profilometry," Optics and Lasers in Engineering 46(2), 106-116 (2008).
[16] Andrae, P., Mieth, U., and Osten, W., "Strategies for unwrapping noisy interferograms in phase-sampling interferometry," 50-60 (1991).
[17] Lamberton, F., Delcroix, N., Grenier, D. *et al.*, "A new EPI-based dynamic field mapping method: Application to retrospective geometrical distortion corrections," Journal of Magnetic Resonance Imaging 26(3), 747-755 (2007).
[18] Liu, X. F., and Prince, J. L., "Shortest Path Refinement for Motion Estimation From Tagged MR Images," Ieee Transactions on Medical Imaging 29(8), 1560-1572 (2010).
[19] Yang, G. Z., Burger, P., Kilner, P. J. *et al.*, "Dynamic range extension of cine velocity measurements using motion-registered spatiotemporal phase unwrapping," Journal of Magnetic Resonance Imaging 6(3), 495-502 (1996).
[20] Huntley, J. M., and Saldner, H., "Temporal Phase-Unwrapping Algorithm for Automated Interferogram Analysis," Applied Optics 32(17), 3047-3052 (1993).
[21] Xiang, Q. S., "Temporal Phase Unwrapping for Cine Velocity Imaging," Jmri-Journal of Magnetic Resonance Imaging 5(5), 529-534 (1995).
[22] Creath, K., and Wyant, J. C., "Absolute measurement of surface roughness," Applied Optics 29(26), 3823-3827 (1990).
[23] Goldstein, G., and Creath, K., "Dynamic four-dimensional microscope system with automated background leveling." 84930N-84930N-11.
[24] Barer, R., "Interference microscopy and mass determination," Nature 169, 366-367 (1952).
[25] Bryan, A. K., Goranov, A., Amon, A. *et al.*, "Measurement of mass, density, and volume during the cell cycle of yeast," Proceedings of the National Academy of Sciences 107(3), 999-1004 (2010).
[26] Davies, H., and Wilkins, M., "Interference microscopy and mass determination," Nature 169, 541 (1952).
[27] Davies, H., Wilkins, M., Chayen, J. *et al.*, "The use of the interference microscope to determine dry mass in living cells and as a quantitative cytochemical method," Quarterly Journal of Microscopical Science 3(31), 271-304 (1954).
[28] Godin, M., Delgado, F. F., Son, S. *et al.*, "Using buoyant mass to measure the growth of single cells," Nature methods 7(5), 387-390 (2010).
[29] Popescu, G., Park, Y., Lue, N. *et al.*, "Optical imaging of cell mass and growth dynamics," American Journal of Physiology-Cell Physiology 295(2), C538-C544 (2008).
[30] Carpenter, A. E., Jones, T. R., Lamprecht, M. R. *et al.*, "CellProfiler: image analysis software for identifying and quantifying cell phenotypes," Genome biology 7(10), R100 (2006).